The Eurasia Proceedings of Science, Technology, Engineering & Mathematics (EPSTEM)
ISSN: 2602-3199

The Eurasia Proceedings of Science, Technology, Engineering and Mathematics (EPSTEM), 2025

Volume 37, Pages 206-222

ICEAT 2025: International Conference on Engineering and Advanced Technology

Structural Performance of High Strength Self-Compaction Concrete Beams with Perforated Expanded Metal Mesh Shear Connectors

Zaineb Ibraheem Saeed
University of Misan

Murtada Abass Abed-Ali
University of Misan

Abstract: This paper displays the results from four shapes of continuous shear connectors made of expanded metal mesh: rectangle, I-shaped, Z-shaped, and truss-shaped. The maximum load that these connectors could withstand under flexural bending was ascertained by testing them through a high-strength concrete beam. Concrete composite units and shear connections are members of a particular class of composite constructions. 24 simply supported beams were tested under two-point bending. A total of 12 beams with one high-strength self-compaction concrete mixture (1:0.91:1.061 ratio mix) and 0.24 water/cement ratio are prepared in one stage in 200 mm x 200 mm x 1200 mm beams, where the results of each group are compared to the other 12 specimens cast in two stages to evaluate the level of composite action between concrete layers due to a change in mechanical properties. The structural behaviour of studied beams, including first crack load, ultimate load, deflection, ductility index, strain characteristics, crack pattern, and failure mode, was investigated. Test results showed beams with shear connectors in a rectangle shape give highlight results in first crack load, ultimate load, deflection at first crack, and ultimate load in addition to the energy absorption (70 kN, 246.66 kN, 1.92 mm,15.41mm, 2124.48 kN.mm, respectively) compared to other types of shear connectors. All beams failed in flexural-shear failure, whereas those with truss connectors exhibited flexural failure. Interface concrete units have influenced all beams that were cast in two stages. Depending on the maximum stress, the types of connectors can be arranged in descending order from rectangle, I, Z, and truss shape.

Keywords: Expanded mesh, HSSCC beam, Continuous shear connector, Failure modes, Types of connectors

Introduction

The construction industry has transformed in recent years, moving away from traditional methods and toward more efficient and organized practices. Composite concrete element production has grown into a specialty in creating concrete products that are lightweight, strong, easy to apply, and cheap, all-in-one materials. The relative light weight compared to high strength is playing the main role, which controls the performance of the structural precast sandwich panel SPSP(Lee et al., 2018; Mahdi et al., 2022). Almost all precast concrete panels currently in use include a composite material, and the stiffness varies based on how the shear connectors are set up (Egbon & Tomlinson, 2021). Shear connections must have the following qualities: resistance to all design forces, ductility in extreme deformation, and sufficient durability. Several techniques have been proposed to determine the type of shear connector that is effective to achieve composite action of the panels, such as continuous steel truss (Bouchair et al., 2012), glass fiber reinforced plastic (Choi et al., 2015), channel (Toghroli et al., 2014), and I-shaped shear connections (Titoum et al., 2016). Shear connectors either concentrated or continuous shear connectors, also known as composite dowels or perforated steel strips, are essential components of composite bridge decks and beams because they offer a continuous

shear connection between a steel beam and a concrete deck. These connections improve the composite action and overall structural performance by forming a continuous connection over the length of the beam, in contrast to standard stud shear connectors, which are discrete (Hechler et al., 2011).

One of the cementitious composites that can satisfy the growing need for complicated, cost-effective, high-performing structures is ferrocement. Ferrocement has unique properties that differ from ordinary reinforcement; when the load increases, ferrocement appears to adjust slowly, becoming more extensible because of the volume fraction and number of layers directly proportional to the elongation (ACI549, 2020). Also, the mesh reinforcement is two-way (transverse and longitudinal), making it a homogeneous-isotropic material, with better shear resistance, and the compressive strength of ferrocement is influenced by the mesh type (square, expanded, or hexagonal) and the properties of the cementitious mortar mix (Malathy &Sasiekalaa, 2012). Ferrocement meshes have been investigated extensively by many researchers. Eltehawy and Shahee (2017) introduces novel precast U-shaped ferrocement forms that are reinforced with different kinds of non-metallic and metallic mesh to determine whether using different kinds of reinforcing meshes as a workable substitute for traditional reinforced concrete slabs in the building of structural slabs with permanent U-shaped ferrocement forms is feasible and effective. Erfan et al. (2021) searched for how ferrocement beams behaved after being exposed to different kinds of ferrocement and ferrocement layers. Alobaidy et al. (2022) studied the shear behavior of hollow ferrocement beams reinforced with different kinds of non-metallic (fiberglass mesh) and metallic (steel wire mesh) reinforcement in self-compacting mortar. All around the world, expanded mesh metal types have been in use for fences, furnishings, and security. Expanded metal mesh systems have been utilized as shear connectors in certain investigations.

One kind of optimal workable mixture that has affected how concrete slabs and beams behave is high-strength self-compacting concrete. HSSCC has been utilized in building and civil engineering projects for many years for its characteristics, such as enabling placement under its weight in heavily reinforced, crowded constructions and/or with complex geometries without the normal requirement for vibrating compaction also the high proportion of fine aggregates, the small size of coarse aggregates, and the action of superplasticizer admixtures, which create the fluidity needed for installation on site, are the key causes of these workability characteristics (Tran et al., 2025). In Portland cement systems, the use of silica fume in percentage by cement weight influences the fresh and hardened properties. From 5% to 15%, silica fume increases the early and design concrete strength and increases the water-binder ratio of mixes with the same workability by up to 30% because of the large specific surface area of its particles (Smirnov et al., 2020) .Silica fume, in compositions with a high level of superplasticizer (1% and more), had a favorable effect on the compressive strength of the concrete at 28 days (Amiruddin et al., 2022).

Any created shear connector is required to understand how it behaves; therefore, experimental tests are needed to provide data by using fully or partially scaled slabs with varying supports or simply supported beams. Thus, two phases were introduced in this paper: the effectiveness and performance of cementitious composites with self-compacting characteristics as structural layers as the first phase, and the stiffest type of innovative expanded mesh continuous shear connectors with flexural behaviour of reinforced concrete beams as the second phase. Four types of shear connectors were proposed to be applied to achieve the maximum load capacity, which could be used with composite panels.

A minimum thickness of the outer layers of concrete sandwich panels of 50 mm is advised; usually, each of the two layers uses the same type of concrete, which may be produced at different locations and assembled in the prefabrication process, making an interface concrete. In the composite cross-section, these units are the weakest area, which could influence the crack pattern and also reduce the ultimate loads and shear resistance even (Halicka, 2011). Since this study is to test the performance of an innovative type of shear connector to be used with a composite insulation concrete slab, two factors were taken into consideration when designing this project: the kind of shear connector and the influence of the interface between the old and kN concrete layers

Materials

Coarse Aggregate (Gravel)

Dry and cleaned aggregate with a maximum size of 10 mm is utilized (ASTM/C33, 2008).

Fine Aggregate (Sand)

Natural sand has been a part of every concrete mixture. 4.75 mm is the maximum grain size ,and the modulus of fineness is 2.71(ASTM/C33, 2008) .

Cement

Ordinary Portland cement (type II) of grade 42.5(ASTM/C150, 2007) was utilized for casting all specimens in this study .

Water of Mixing

Every specimen was cast using water that had undergone reverse osmosis (R.O.) treatment.

Superplasticizer and Silica Fume

10% silica fume has been used in place of some cement in concrete (ASTM/C1240, 2003). 2% superplasticizer of type ViscoCrete-171 Precast (3rd Generation)(ASTM/C494, 2005) was used for the purpose of reducing the percentage of water content for concrete mixtures.

Reinforcing Steel

Steel bars of grade(60) diameter of Ø10 mm without stirrups used for the reinforcement of beam specimens were Fy = 464.3 MPa and Fu = 579.9 MPa (ASTM/A615, 2012) (ASTM A615/A615M, 2012).

Expanded Metal

Standard type, overlapped, and diamond shape. Thickness of 3 mm, LW (50.8 mm), SW (22 mm), yield strength of 310 MPa, and ultimate tensile strength of 420 MPa (ACI549, 2020) .

Steel Angle

Metal right angles thickness of 2 mm and Fu = 519 MPa (ASTM/A370, 2007) were used to connect each corner from the top and inside along the connector.

Experimental Program: Phase I

Mixture of Concrete

All specimens for the study were cast by using self-compacting concrete with a high-strength cube compressive strength of more than 70 MPa under (IS10262, 2019). Following the IS standard, the first step is choosing the required grade of concrete; then maximum sizes of aggregate are subsequently taken into consideration while determining the water-to-cement ratio. Numerous attempts have been made to determine the optimal dosage of silica fume and superplasticizer with an aggregate size of 10 mm. High concentrations of chemical admixtures and silica fume (10% and 2%) were used to optimize the concrete mix. Based on the outcomes of experimental attempts, the water ratio was lowered to 24.5%. A 40 L pan mixer was used to mix the mixtures. After adding silica to the cement, it was mixed for two minutes. Following the automatic mixing method according to the specification (ASTM/C192, 2019) ,dry sand was then slowly placed over the cementitious material and mixed for three minutes. Equal parts water and superplasticizer-171 were mixed and added to the admixture, followed by the remaining water and superplasticizer at

the maximum speed of the mixer. The gravel was then added to the mixture and allowed homogenize for three minutes before the cubes, cylinders, and prisms were poured. All material amounts of concrete mix are in (Table 1).

Table1.High strength SCC mix by weight

Concrete Mix	Cement (kg/m3)	Sand (kg/m3)	Gravel (kg/m3)	Water (L)	Content	Silica Fume (kg/m3)	Superplasticizer (L)
	802.14	726.9	851.3	219.48		89.12	17.8

Characteristics of High Strength SCC

The fresh form features of high-strength SCC were examined. The time it takes for the concrete to reach a 500mm diameter is 4 seconds, recorded during the slump flow test, which recorded 770mm (BS12350-8, 2010). The concrete's capacity to pass the J-ring test is recorded at 8mm (BS12350-12, 2010) .About 12 liters of concrete are poured into the V-funnel, and the amount of time it takes for the concrete to pass through the device is 18 seconds (BS12350-9, 2010). Tests for compressive Fcu, flexural Fr, and splitting tensile strength Ft were used to examine HSSCC in the hardened state (ASTM/C39, 2009) , (ASTM/C78, 2018), and (ASTM/C496, 2006) respectively .All results are shown in (Table 2).

Table 2. Test results of compressive strength splitting tensile and flexural strength

No.	Compressive Strength Fcu (MPa)				Splitting strength Fr (MPa)	Flexural strength Ft (MPa)
	3 day	7 day	28 day	56 day	28 day	28 day
1	53.6	60.3	74.7	76.7	13.53	7.26
2	54.7	59.4	68.3	74.13	14.98	7.28
3	46.5	49.7	73.6	81.6	14.4	7.23
Avg.	51.6	56.46	72.2	77.47	14.3	7.25

Experimental Program: Phase II

Beam Details

All beams were designed as single reinforcement solid sections according to (ACI318-14, 2014). The total length for all beams was 1200 mm, the width was 200 mm, and the total depth was 200 mm; also, each beam has the same compressive strength and the same bottom reinforcement of 2Ø10 mm. To determine whether the beams with shear connectors will develop shear strength from the post-cracking tensile strength under their maximum load, beams were designed with the minimum code-permitted steel reinforcement ratio and without stirrups (Figure 1).

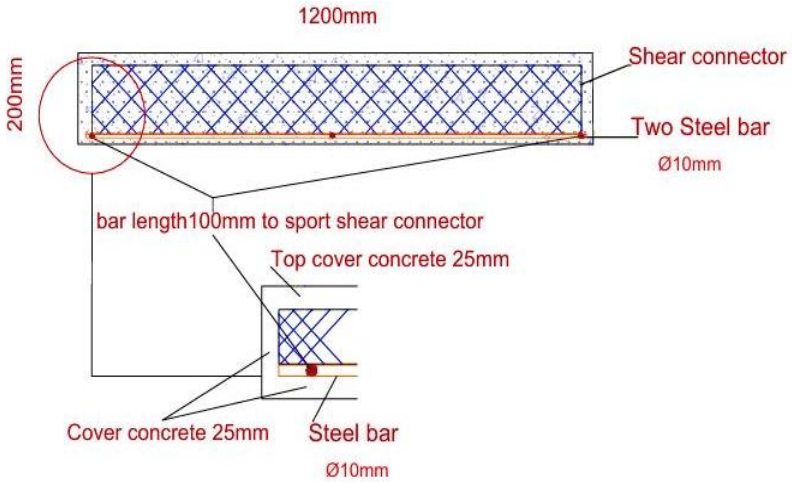

Figure 1. Beams geometric shape

Four types of continuous connectors run the full length of the beam: rectangle section, I-section, Z-section, and truss shape (Figure 2). The dimensions were taken according to (ANSI/AISC, 2005). Because of the impossibility of nailing, screwing, or welding, each section of shear connectors was made by cutting expanded sheet metal with an electric angle grinder to the dimensions shown in the details of (Figure 3).

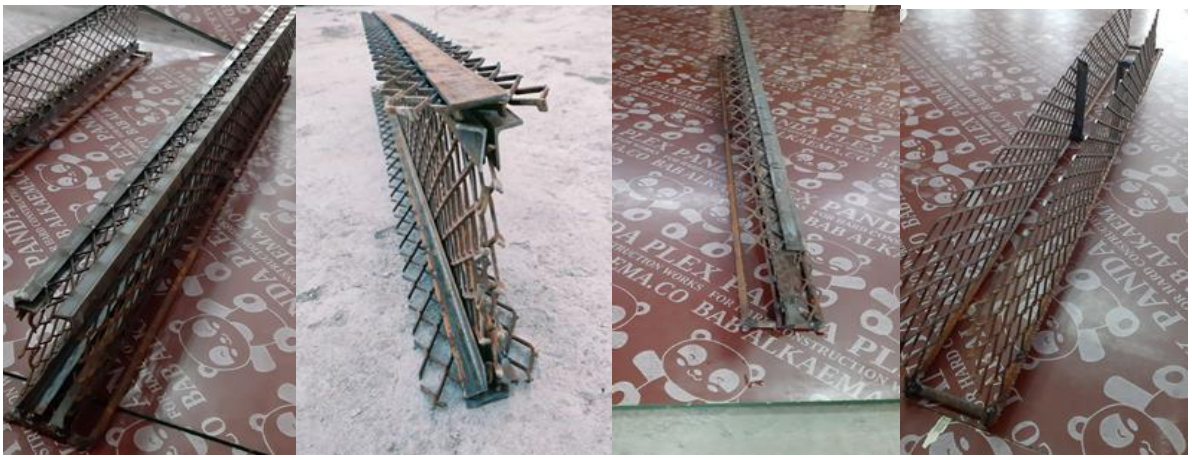

(a)Rectangular (b)I-shape (c) Z-shape (d)Truss- shape

Figure 2. Types of shear connectors

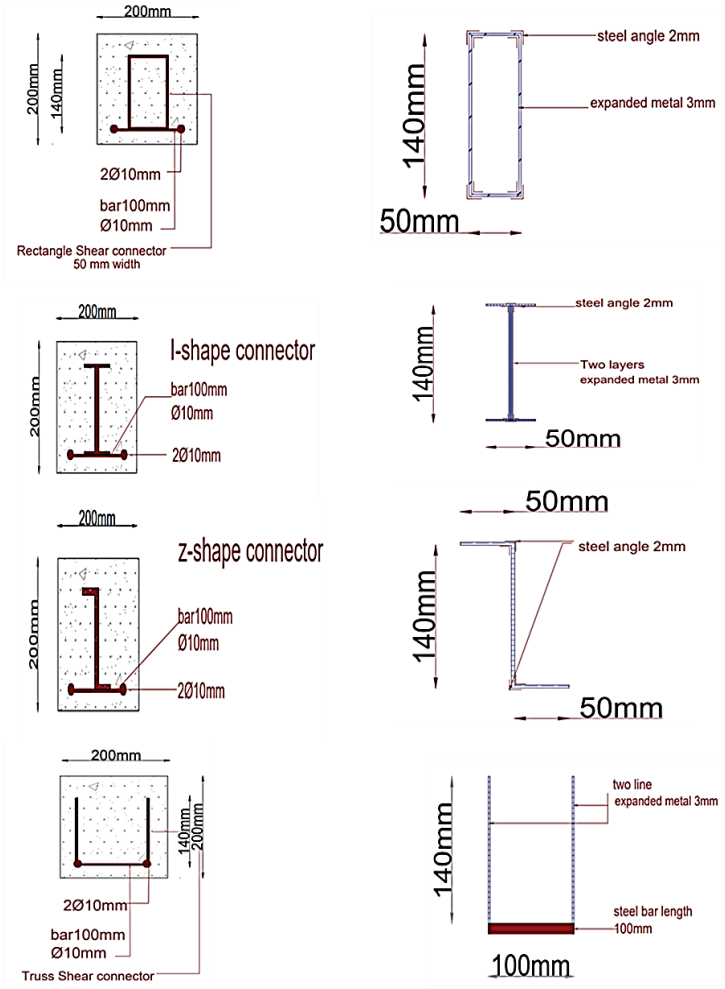

Figure 3. Shear connectors details

To form the required structural element, each meeting edge was connected with another by stick welding, and then a steel angle from the top and inside was welded along the connector. Shear connectors were related to the reinforcement steel using a cross-section steel Ø10mm with a length of 100mm to fix the shear connector over the rebar and also prevent movement. Two truss connectors were welded directly on the rebar, and an angle steel was added in the middle as vertical stiffeners. In the symbolization of the specimens, for example (AR1), the first letter indicates the group, the next letter represents the type of shear connector, and the last digits define the numbers of the beam specimens (Table 3).

Table 3. Details of beams with shear connectors

Specimens	Casting	Type of shear connectors	Tension steel bars	Dimension mm	Finding
AR1, AR2, AR3 BR1, BR2, BR3	One stage Two stages	Rectangular	2Ø10	1200X200X200	All groups A: 1- Average ultimate load
AI1, AI2, AI3 BI1, BI2, BI3	One stage Two stages	I-shape	2Ø10	1200X200X200	2- Stiffness, ductility 3- Failure mode
AZ1, AZ2, AZ3 BZ1, BZ2, BZ3	One stage Two stages	Z-shape	2Ø10	1200X200X200	All groups B: 1- Average ultimate load
AT1, AT2, AT3 BT1, BT2, BT3	One stage Two stages	Truss- shape	2Ø10	1200X200X200	2- Stiffness, ductility 3- Failure mode 4- Influence of concrete interface

Casting Procedure and Curing of Beam Specimens

Shear connectors with bars were placed inside the molds, and plastic spacers were used to maintain the cover of concrete and to keep the right position of reinforcement during the casting of concrete. 12 beams were regarded as an A team, completely cast, representing reference models, and to simulate the thickness of concrete slab layers and to study the effect of the composite action resulting from the interface between the old and new concrete, 12 further specimens were cast to a thickness of barely 50mm, and a day later, they were completely cast (Figure 4). As a collective, they were as B team. The treatment consisted of moistening the upper surface only without a binding agent. Each connector type was tested in 3 models from group A and 3 models from group B. The casting procedure was done without compaction for all specimens. The curing of the cast specimens was done by the normal methods of curing by sprinkling water and keeping the elements moist for 28 days using wet burlap. The models were also covered using thick nylon (Figure 4).

Figure 4. Casting of beam specimens and curing

Test Setup for Beams

The test method covers the determination of the flexural strength of a reinforced concrete beam with two-point loading by using an automated 600 kN compression machine according to (ASTM/C78, 2018). The vertical position of the loading and support blocks was maintained. The beams had a 1000 mm clear span; an LDVT with a 100 mm sensor was used to record the deflection at the beam mid-span (Figure 5). The deflection readings were captured using a portable electronic data logger. The load was applied at a rate of 1 MPa/min. As the loading increased, the crack patterns were noted and observed

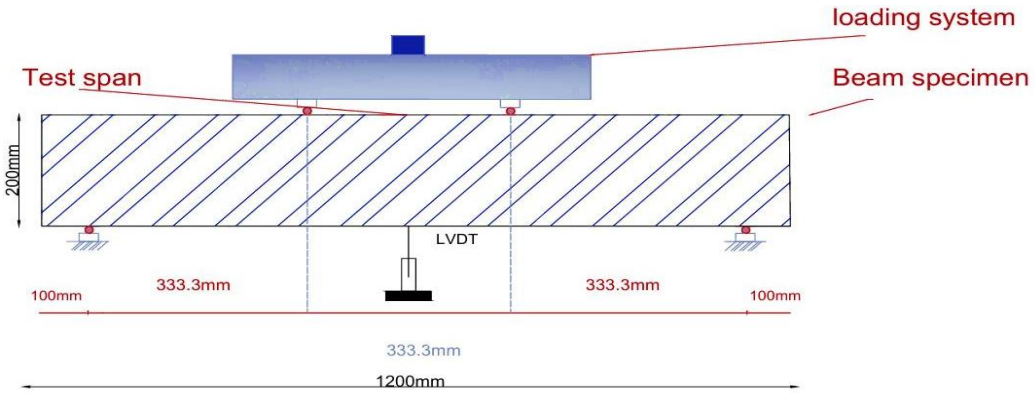

Figure 5. Test set-up for beam specimens

Results and Discussion

Results For Phase II

Beams with shear connectors are studied through the first crack load, ultimate load, ductility, failure mode, load-deflection relationships. All test data were displayed in (Table 4).

Table 4. Second phase experimental results for load, deflection and failure mode

Specimens	First Crack Load, Pcr (kN)	Deflection At First Crack Load, Δcr(mm)	Ultimate Load, Pu (kN)	Deflection At Ultimate Load Δmax(mm)	Failure Mode
AR1	60	1.688	264	15.28	Flexural, Shear
AR2	75	2	230	14.62	Flexural ,Shear
AR3	75	2.108	246	16.34	Flexural ,Shear
BR1	70	1.027	219	9.50	Flexural .Shear
BR2	70	0.98	205	8.12	Flexural .Shear
BR3	70	1.416	212	8.72	Flexural ,Shear
AI1	50	1.415	216	7.22	Flexural ,Shear
AI2	65	1.04	195	7.42	Flexural ,Shear
AI3	65	1.132	235	9.64	Flexural ,Shear
BI1	55	1.09	190	7.31	Flexural ,Shear
BI2	55	1.08	207	8.21	Flexural ,Shear
BI3	50	0.97	190	7.53	Flexural ,Shear
AZ1	60	1.311	175	8.94	Flexural ,Shear
AZ2	60	1.861	151	7.95	Flexural ,Shear
AZ3	65	1.72	181	9.12	Flexural ,Shear
BZ1	45	1.22	164	8.01	Flexural ,Shear
BZ2	45	1.25	174	9.83	Flexural ,Shear
BZ3	55	1.15	187	8.65	Flexural ,Shear
AT1	45	1.55	131	7.86	Flexural
AT2	45	1.07	135	7.989	Flexural
AT3	55	1.59	136	7.95	Flexural
BT1	40	1.08	130	6.73	Flexural
BT2	35	1.03	123	5.21	Flexural
BT3	40	1.07	128	5.98	Flexural

Ductility

The concept of "ductile design" refers to a structural system's capacity to guarantee that specified zones, referred to as "plastic hinges," with limited displacements and a specific length are capable of developing deformations in response to strong seismic action and preventing the collapse of the structure Additionally, by limiting lateral displacement, ductility helps control the structural system's response to seismic action and prevents the possibility of non-economic structure design. The ductility index is expressed as a ratio of the displacement corresponding to the global yielding of the structure (Δy) to the ultimate displacement of the system (Δmax).Equation 1 can be used to determine ductility index (Abdulraheem, 2018). (Table 5) presents the ductility of all beams in terms of the ductility index.

$$\mu = \frac{\Delta u\ max}{\Delta y} \tag{1}$$

Energy Absorption and Initial Stiffness

Energy absorption is an increasingly important function of structure and materials and an important requirement in design. A material or structure absorbs energy, often from an external impact, and dissipates it through mechanisms like plastic deformation or fracture. Energy absorption can be calculated by the total area under the load-deflection curve. Initial stiffness is a crucial concept in structural analysis, specifically in direct displacement-based design for seismic analysis. It essentially represents the slope of the load-deformation curve of a structure or a joint under initial, linear elastic loading. The load-deflection relationship can be used to define the yield point by the yield strength and yield displacement; initial stiffness can be calculated by equation 2 (Sullivan et al., 2004). The initial stiffness of second-phase specimens and energy absorption are shown in (Table 5).

$$\text{Initial Stiffness} = \frac{Py}{\Delta y} \tag{2}$$

Table 5. Initial stiffness, energy absorption, ductility index, tensile and compressive strain

Specimens	Initial Stiffness (kN/mm)	Energy Absorption (kN.mm)	Ductility Index	Yield Deflection Δy(mm)	Yield Load Py(kN)
AR1	17.27	2233.98	2.05	7.42	128.28
AR2	15.73	1956.94	2.38	6.13	96.48
AR3	15.05	2182.52	2.36	6.91	104.06
BR1	23.03	1213.24	2.95	3.21	74
BR2	25.21	997.36	2.83	2.87	72.37
BR3	24.303	1126.17	2.03	4.28	104.22
AI1	29.904	772.87	2.49	2.89	86.55
AI2	26.24	750.29	2.36	3.13	82.28
AI3	24.37	1088.71	2.35	4.09	99.73
BI1	25.95	783.43	1.94	3.76	97.75
BI2	25.21	933.32	2.02	4.06	102.47
BI3	25.22	824.8	2.04	3.68	92.98
AZ1	19.56	797.47	2.33	3.82	74.8
AZ2	18.97	625.47	1.69	4.68	88.87
AZ3	19.84	837.43	1.90	4.78	95.04
BZ1	20.46	702.53	1.80	4.44	91.01
BZ2	17.68	938.17	2.03	4.83	85.49
BZ3	21.61	822.94	2.21	3.91	84.52
AT1	16.66	188.23	1.74	4.51	75.2
AT2	16.89	204.19	2.48	3.21	54.24
AT3	17.10	204.83	2.02	3.93	67.24
BT1	19.30	169.31	1.91	3.51	67.77
BT2	23.61	114.69	1.43	3.61	85.47
BT3	21.40	142.23	1.74	3.42	73.3

Beams in Group A and B with Rectangular Shear Connector

A total of six beams is investigated under two-point bending from groups AR and BR. Both series AR and BR had a linear load-deflection relationship, where the first flexural cracking of AR appeared at an average displacement of 1.92 mm; after that, deflection increased as the load increased to the ultimate load with an average maximum displacement of 15.41mm (Figure 6).

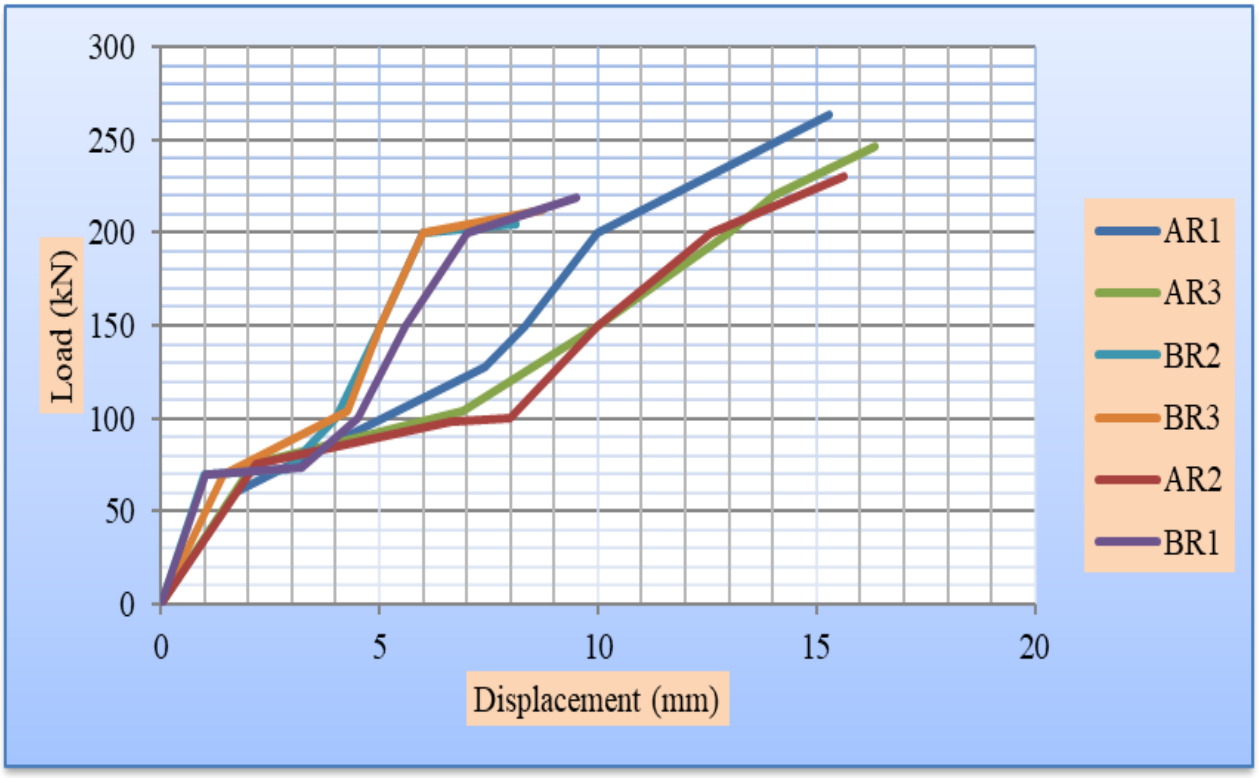

Figure 6. Load-deflection relationship for series AR, BR beams

There is a clear difference in the diagram in the displacements of group B, where the maximum displacement rate reached 8.78 mm. All beams developed enough cracks before failure. The transverse force is initiating, causing diagonal cracks. Thus, it can be stated that all the beams were destroyed due to the shear in the support zones (Figure 7). In BR3, after the crack pattern reaches the interface, after a short propagation along the interface, it appears in the upper layer, and the failure is caused by exceeding the shear resistance of the beam; also, the partial separation with a vertical crack of the edge of the model is observed in the lower layer (Figure 8). This behavior was observed in composite beams with a low ratio of transverse reinforcement, in which the height of the upper layer was greater than the height of the lower layer (Halicka, 2011).

All concrete beams reach high resistance, which may be attributed to the resistance of the concrete or because of the rectangular cross-section, orientation, and volume fraction of expanded mesh. The average first crack load is 70 kN for all beams. For the specimens (AR1, AR2, AR3), which represent the control specimens poured at the same time completely, the obtained experimental failure load on average, Pu is 246.66 kN. For specimens (BR1, BR2, and BR3), the average failure load was 212 kN.

The superiority of the first group in terms of maximum displacement and load may be attributed to the lack of cohesion in composite concrete layers in group BR (Halicka, 2011). It is noted in two-stage casting without using adhesion or stirrups between concrete layers that the models BR are decreasing in ultimate load, maximum deflection, and energy absorption by 16.35%, 75.5%, and 91%, respectively. The initial stiffness and ductility index values for group A are lower than group B by 51% and 15%, because the deflection and load at the yield point for A are greater than B.

Figure 7. Crack pattern of beams with rectangle shear connector

Figure 8. Slip concrete lower layer in BR3 beam

Beams in Group A and B With I- Shape Shear Connector

For the second series of beams, (Figure 9) shows all the readings recorded during the test, where the first crack was at an average reading of 1.19 mm and 1.04 mm, and the average higher readings were 8.09 mm and 7.68 mm for groups AI and BI, respectively. All beams failed due to imbalance because of shear forces (Figure 10). The same behaviour was observed in BI1: the crack moves through the interface and into the point load of the beam before moving on to the upper layer, causing a slip at the end of the beam (Figure 11).

Due to bonding new concrete to old concrete in the second series BI, this influences the mechanical characteristics of the members (Halicka, 2011). First crack and ultimate load, first crack and maximum displacement, energy absorption, ductility index, and initial stiffness averages for AI are higher by 11.16%, 9.13%, 12.6%, 5%, 2.7%, 17.9%, and 5.5%, respectively, indicating that group AI is more controlled than BI.

Although it has less load resistance, an I-section connector with a beam has more stiffness. While AI series are 14.5% less resistant to stress than AR series, they are 40% more resistant to elastic deformations and 5.8% more resistant to inelastic deformations. As for the BR group, BI is 5% more stiff and less resistant to load and plastic deformations by 8.34% and 32%, respectively.

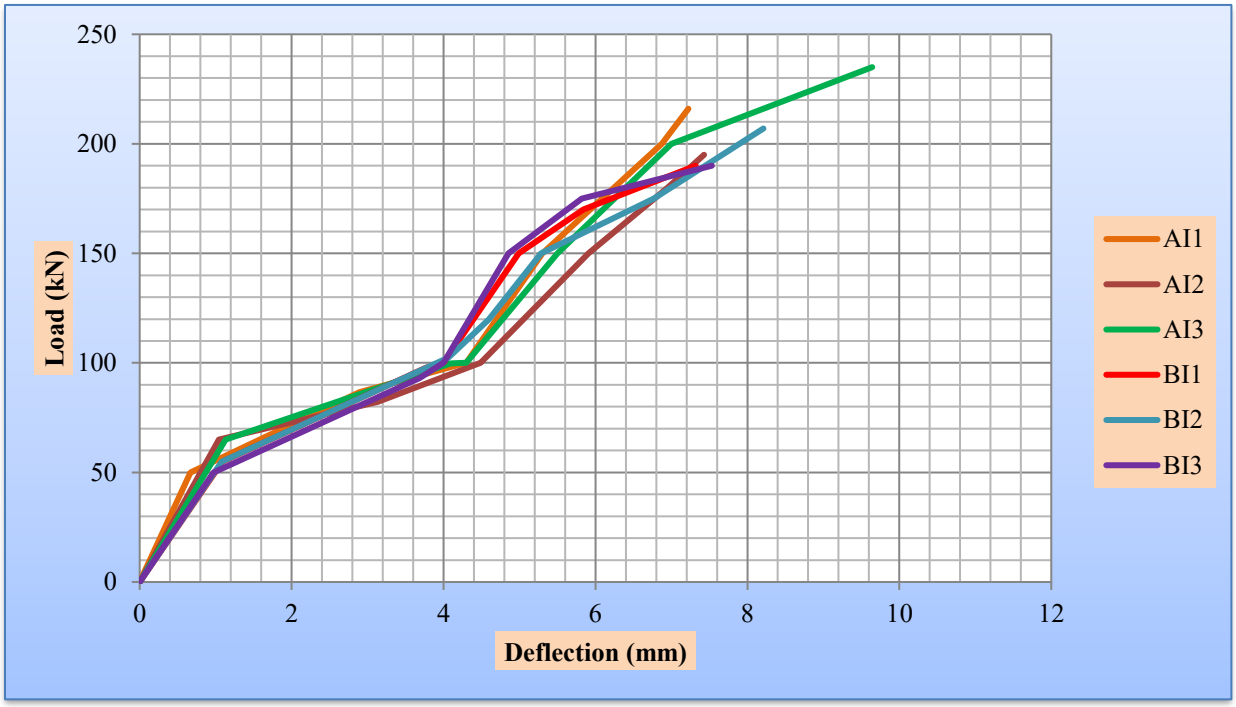

Figure 9. Load-deflection relationship for series AI, BI beams

Figure 10. Slip concrete layer in BI1 beam

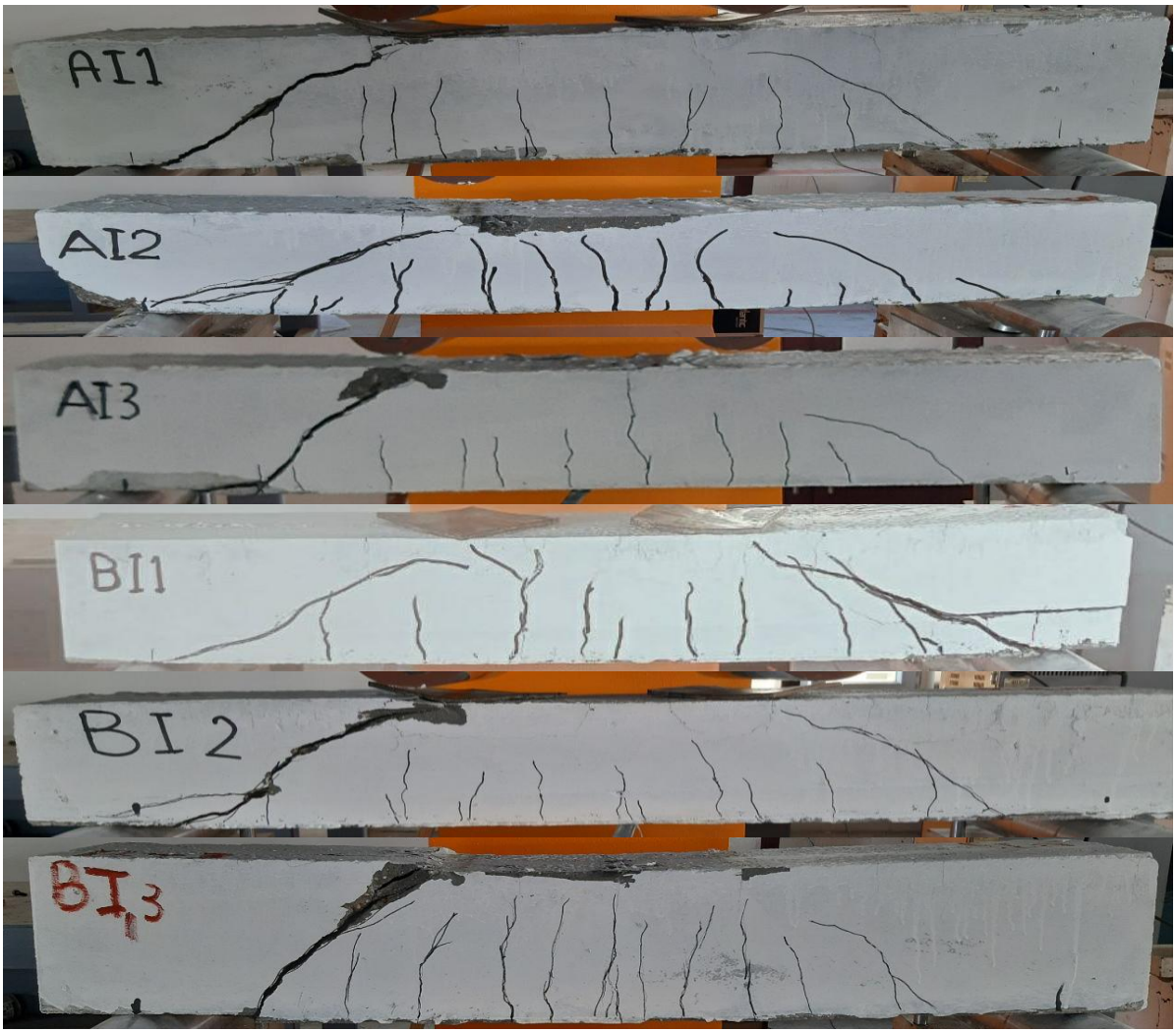

Figure 11. Crack pattern of beams with I-shear connector

Beams in Group A and B with Z- Shape Shear Connector

For the third type of shear connector (Figure 12), the deflections of the beams were approximately the same from before the first crack load to the yielding point until the ultimate loads, with the same crack pattern and failure mode as prior beams with rectangular and I-shaped connectors (Figure 13).It also shows in beam BZ1 that the bottom layer was subjected to separation because of the lack of cohesiveness in the composite concrete layers in group BZ.

In this group, the average of first crack deflection and first crack load for AZ is more than BZ by 21.6% and 26.4%, respectively. It noted a difference in the average ultimate load in beams AZ ,which is lower than that in beams BZ by 3.55%; despite the convergence of the values of the two beams, AZ3 and BZ3 were 181 kN and 187 kN, respectively; perhaps the cause is due to the large amount of cementitious materials in high-performance concrete mixtures, which causes an increase in the temperature of the concrete during hydration, which leads to an increase in resistance for group BZ (Carrasquillo, 2000). Because the yield load is more than AZ by 0.91 %, it appears in ductility, initial stiffness, and energy by 2%, 2.3%, and 8.25%, respectively.

Compared to the rectangular section, beams with shear connectors of Z-shape have less load capacity and less ductility. The AZ group reduced the concrete beams' load resistance by 45% and reduced their ductility by 14.7% but increased their stiffness by 17.6 % concerning AR. BZ reduced beams' stiffness, load resistance, and ductility by 21.4%, 21%, and 29.4%, respectively, with respect to BR.

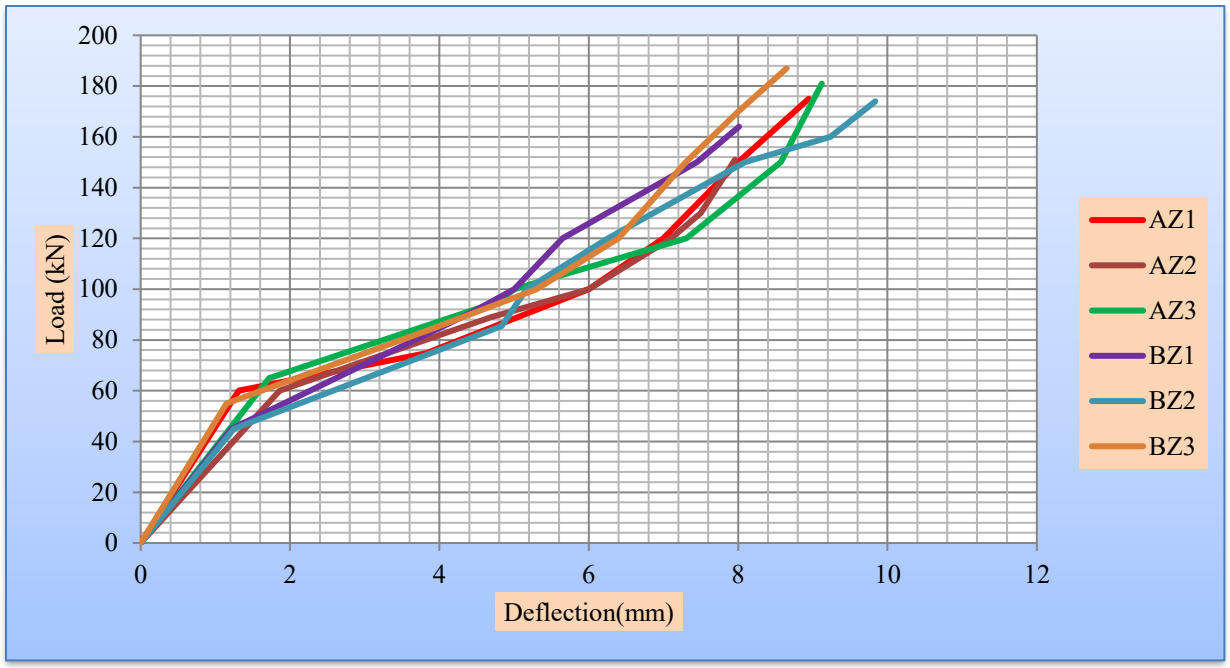

Figure 12. Load-deflection relationship for series AZ, BZ beam

Figure 13. Crack pattern of beams with Z- shear connector

Beams in Group A and B with Truss- Shape Shear Connector

In the last series where truss-shaped shear connectors were used, these specimens exhibited a crack pattern different from that of the previous ones. Series AT, with an average maximum displacement of 7.93 mm, failed in flexure at the average ultimate load of 134 kN. Also, series BT of beams failed in flexure, as shown by vertical cracks in the middle of the specimens (Figure 14) at a load and deflection 5.5% and 32.8% lower than series AT; this difference between the two groups also comes from the influence of casting concrete layers at different times. The load-deflection relationship is shown in (Figure15).

The maximum load rates were lower than those with other shear connectors, possibly due to the thin section of expanded mesh or the number of connectors used. These beams from the AT and BT series are less ductile and have a lower load capacity than the beams of rectangular connectors. In terms of AR, the AT group increased the concrete beams' stiffness by 5.15 percent while decreasing their ductility by 8.7 percent and their load resistance by 84%. In comparison to BR, BT decreased the ductility, load resistance, and stiffness of beams by 52%, 67%, and 12.8%, respectively.

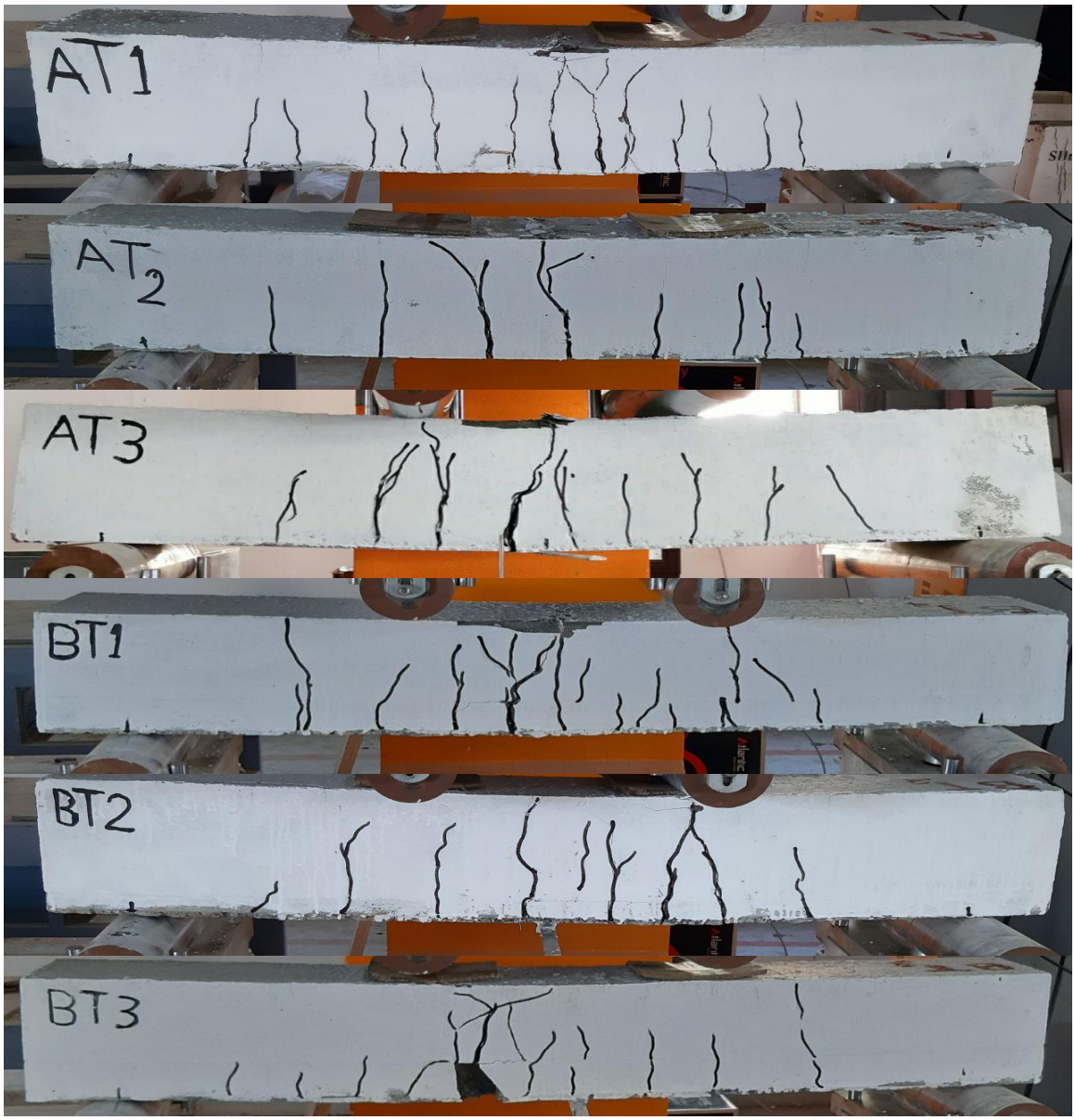

Figure 14. Crack pattern of beams with truss- shear connector

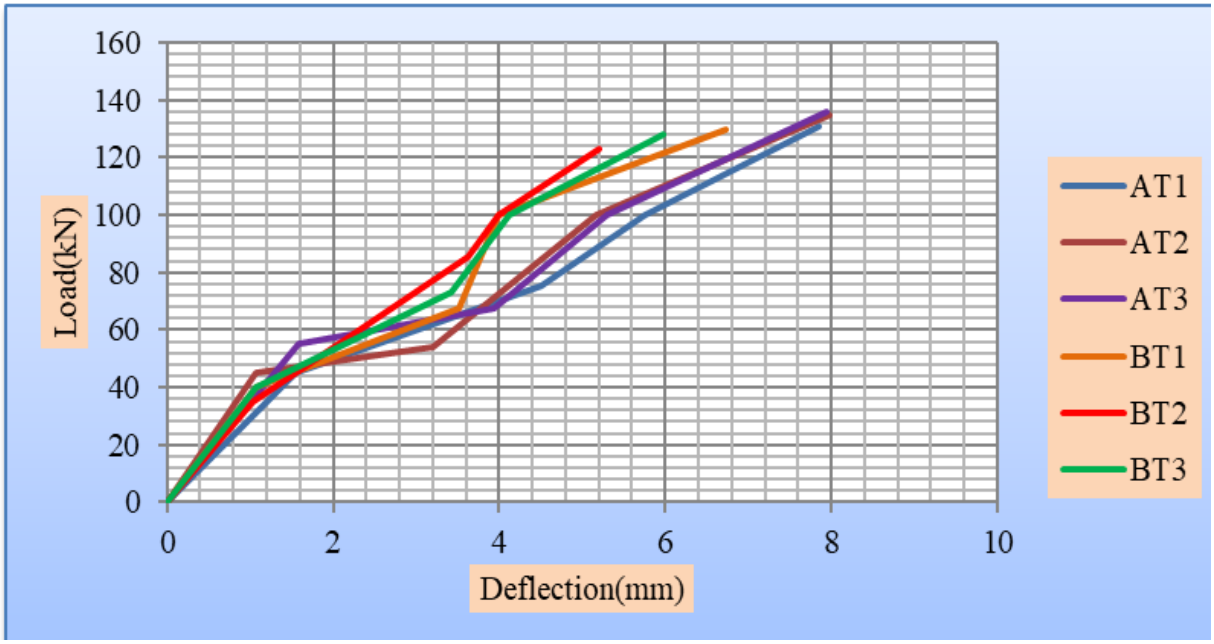

Figure 9. Load-deflection relationship for series AT, BT beams

Conclusions

The recommended mix design offered high strength and workability, as evidenced by qualities both fresh and hardened that are comparable to the standard IS guidelines. The optimal mix consists of 2% superplasticizers and 10% replacement cement with silica fumes that may be used for strengthening, repairing, maintaining, and retrofitting reinforced concrete structures. In addition, it can be applied to ferrocement. For the same concrete strength, the current study found that the cross-section of the connector type affects the maximum load as well as the bond between the concrete joints. Based on the previous results and depending on the maximum stresses, the types of connectors can be arranged in descending order from rectangle, I, Z, and truss shape. For reinforced concrete beams, the innovative expanded wire mesh shear connectors in a rectangle shape give higher results in first crack load, ultimate load, the displacement ductility, and energy absorption than other types of shear connectors. The reinforced beams with the proposed shear connector are capable of exhibiting deformation characteristics comparable to that of steel reinforced beams before failure, this can be attributed to the elastic plastic behaviour of steel and ferrocement. Although the failure pattern in beams with a truss-shaped connector is different compared to other types, the cracks that occurred as a result of loading are considered a sufficient indicator to warn of the seriousness of the situation for the structure. However, by adding greater shear reinforcement, it addresses the issues with the support zones in these units. The appearance of one model in each group subjected to separation in the concrete layers indicates the interface's impact on the composite concrete units' resistance. To estimate the bond strength, it is required to use suitable repair materials or use mechanical treatments and take special care in curing. Because cementitious materials make up a large amount of concrete, temperature development has a significant impact on the performance of the beams.

Scientific Ethics Declaration

* The authors declare that the scientific ethical and legal responsibility of this article published in EPSTEM journal belongs to the authors.

Conflict of Interest

* The authors declare that they have no conflicts of interest

Funding

* Without funding

Acknowledgements

*This article was presented as an oral presentation at the International Conference on Engineering and Advanced Technology (ICEAT) held in Selangor, Malaysia on July 23-24, 2025.

*The authors gratefully thank the support provided by the laboratory of the Technical Institute of Amara and the Department of Civil Engineering at University of Misan.

Reference

Abdulraheem, M. S. (2018). Experimental investigation of fire effects on ductility and stiffness of reinforced reactive powder concrete columns under axial compression. *Journal of Building Engineering, 20*, 750–761.

American Concrete Institute. (2014). *Building code requirements for structural concrete (*ACI 318-14). Retrieved from https://www.concrete.org/Portals/0/Files/PDF/Previews/318-14_preview1.pdf

American Concrete Institute. (2020). *Guide to design and construction of externally bonded fabric-reinforced cementitious matrix and steel-reinforced grout systems for repair and strengthening of concrete structures* (ACI 549). American Concrete Institute

Alobaidy, Q. K. N. A., Abdulla, A. I., & Al-Mashaykhi, M. (2022). Shear behavior of hollow ferrocement beam reinforced by steel and fiberglass meshes: Shear behavior. *Tikrit Journal of Engineering Sciences, 29*(4), 27–39.

Amiruddin, A., Ibrahim, I., Sulianti, I., Subrianto, A., Ramadhan, M., & Khuljanna, T. K. (2022). Flexural strength of self-compacting concrete beams. In *5th FIRST T1 T2 2021 International Conference (FIRST-T1-T2 2021).*

American Institute of Steel Construction. (2005). Specification for structural steel buildings (ANSI/AISC 360-10). Retrieved from https://www.aisc.org

ASTM International. (2007). *Standard test methods and definitions for mechanical testing of steel products* (ASTM A370). Retrieved from https://www.astm.org

ASTM International. (2012). *Standard specification for deformed and plain carbon-steel bars for concrete reinforcement* (ASTM A615). Retrieved from https://www.astm.org

ASTM International. (2008*). Standard specification for concrete aggregates* (ASTM C33). Retrieved from https://www.astm.org

ASTM International. (2009). *Standard test method for compressive strength of cylindrical concrete specimens* (ASTM C39). Retrieved from https://www.astm.org

ASTM International. (2018). *Standard test method for flexural strength of concrete (using simple beam with third-point loading)* (ASTM C78). Retrieved from https://www.astm.org

ASTM International. (2007). *Standard specification for Portland cement* (ASTM C150). Retrieved from https://www.astm.org

ASTM International. (2019). *Standard practice for making and curing concrete test specimens in the laboratory* (ASTM C192). Retrieved from https://www.astm.org

ASTM International. (2005). *Standard specification for chemical admixtures for concrete* (ASTM C494). Retrieved from https://www.astm.org

ASTM International. (2006). *Standard test method for splitting tensile strength of cylindrical concrete specimens* (ASTM C496). Retrieved from https://www.astm.org

ASTM International. (2003). *Standard specification for silica fume used in cementitious mixtures* (ASTM C1240). Retrieved from https://www.astm.org

Bouchair, A., Bujnak, J., & Duratna, P. (2012). Connection in steel–concrete composite truss. *Procedia Engineering, 40*, 96–101.

British Standards Institution. (2010). *Testing fresh concrete: Self-compacting concrete—Slump flow test* (BS EN 12350-8). British Standards Institution.

British Standards Institution. (2010). *Testing fresh concrete: Self-compacting concrete—V-funnel test* (BS EN 12350-9). British Standards Institution

British Standards Institution. (2010). *Testing fresh concrete: Self-compacting concrete—J-ring test* (BS EN 12350-12). British Standards Institution

Carrasquillo, J. J. M., & R. L. (2000). Influence of hydration temperature on durability and mechanical property performance of prestressed and precast high-performance concrete beams. *Transportation research record, 1696*(1), 131-142.

Choi, K. B., Choi, W. C., Feo, L., Jang, S.-J., & Yun, H.-D. (2015). In-plane shear behavior of insulated precast concrete sandwich panels reinforced with corrugated GFRP shear connectors. *Composites Part B: Engineering, 79*, 419–429.

Egbon, B., & Tomlinson, D. (2021). Experimental investigation of longitudinal shear transfer in insulated concrete wall panels with notched insulation. *Journal of Building Engineering, 43*, 103173.

Halicka, A. (2011). Influence of new-to-old concrete interface qualities on the behaviour of support zones of composite concrete beams. *Construction and Building Materials, 25*(10), 4072–4078.

Hechler, O., Berthellemy, J., Lorenc, W., Seidl, G., & Viefhues, E. (2011). Continuous shear connectors in bridge construction. In *composite construction in steel and concrete VI* (pp. 78–91).

Bureau of Indian Standards. (2019). *Concrete mix proportioning—Guidelines* (IS 10262:2019). Bureau of Indian Standards

Lee, J. H., Kang, S.-H., Ha, Y., & Hong, S.G. (2018). Structural behavior of durable composite sandwich panels with high performance expanded polystyrene concrete. *International Journal of Concrete Structures and Materials, 12*, 1–13.

M. Erfan, A., H. K. Elafandy, T., M. Mahran, M., & Said, M. (2021). Behavior of self-compacted concrete ferrocement beams. *Journal of Engineering Research and Reports, 21*(1), 1–14.

Mahdi, S., Sheikh, A., Ali, M. M., & Elchalakani, M. (2022). Experimental investigation into the structural behaviour of ultra-high performance fibre-reinforced concrete box-celled composite panels. *Composites Part C: Open Access, 9*, 100329.

Sasiekalaa, K., & Malathy, R. (2012). A review report on mechanical properties of ferrocement with cementitious materials. *International Journal of Engineering Research & Technology, 1*(9), 9432

Shaheen, Y. B., & Eltehawy, E. A. (2017). Structural behaviour of ferrocement channel slabs for low cost housing. *Concrete Research Letters, 8*(2), 48-64.

Smirnov, A., Dobshits, L., & Anisimov, S. (2020). Effect of superplasticizer and silica fume on the properties of self-compacting mortars. *IOP Conference Series: Materials Science and Engineering.*

Sullivan, T., Calvi, G., & Priestley, M. (2004). Initial stiffness versus secant stiffness in displacement based design. In *13th World Conference on Earthquake Engineering (WCEE).* Retrieved from https://nicee.org

Titoum, M., Mazoz, A., Benanane, A., & Ouinas, D. (2016). Experimental study and finite element modelling of push-out tests on a kN shear connector of I-shape. *Advanced Steel Construction, 12*(4), 487–506.

Toghroli, A., Mohammadhassani, M., Suhatril, M., Shariati, M., & Ibrahim, Z. (2014). Prediction of shear capacity of channel shear connectors using the ANFIS model. *Steel and Composite Structures, 17*(5), 623–639.

Tran, T.-H., Le, A.-T., & Pham, D.-T. (2025). Review of UHPC concrete mixture's ability to use recycled, by-product, waste, or locally sourced materials. *Transportation Research Procedia, 85*, 191–198.

Author(s) Information

Zaineb Ibraheem Saeed
College of Civil Engineering, University of Misan
Misan, Iraq
Contact e- mail:*aenghrc.2211@uomisan.edu.iq*

Murtada Abass Abed-Ali
College of Civil Engineering, University of Misan
Misan, Iraq

To cite this article:

Saeed, Z.I., & Abed-Ali, M.A. (2025). Structural performance of high strength self-compaction concrete beams with perforated expanded metal mesh shear connectors. *The Eurasia Proceedings of Science, Technology, Engineering and Mathematics (EPSTEM), 37,* 206-222.